LA-UR- 09-03686

*Approved for public release;*
*distribution is unlimited.*

| | |
|---|---|
| *Title:* | Near-Field Effects of Asteroid Impacts in Deep Wtaer |
| *Author(s):* | Galen Gisler, Robert Weaver and Michael Gittings |
| *Intended for:* | Conference on Submarine Mass Movement and their Consequences, Austin TX November 2009 |




Form 836 (7/06)

# Near-Field Effects of Asteroid Impacts in Deep Water

**Galen Gisler[1], Robert Weaver[2], and Michael Gittings[3]**

*[1]Physics of Geological Processes, University of Oslo*
*PO Box 1048 Blindern, 0316 Oslo, NORWAY*
*email: galen.gisler@fys.uio.no*

*[2]Los Alamos National Laboratory*
*MS T086, Los Alamos, New Mexico 87545, USA*
*email: rpw@lanl.gov*

*[3]Science Applications International*
*MS T086, Los Alamos, New Mexico 87545, USA*
*email: gitting@lanl.gov*

## Abstract

Our previous work has shown that ocean impacts of asteroids below 500 m in diameter do not produce devastating long-distance tsunamis. Nevertheless, a significant portion of the ocean lies close enough to land that near-field effects may prove to be the greatest danger from asteroid impacts in the ocean. Crown splashes and central jets that rise up many kilometres into the atmosphere can produce, upon their collapse, highly non-linear breaking waves that could devastate shorelines within a hundred kilometres of the impact site. We present illustrative calculations, in two and three dimensions, of such impacts for a range of asteroid sizes and impact angles. We find that, as for land impacts, the greatest dangers from oceanic impacts are the short-term near-field, and long-term atmospheric effects.

## I. Introduction

Oceans cover three-quarters of the Earth's surface, yet geological evidence for deep ocean impact events is scarce. Tectonic subduction has wiped away essentially all of the oceanic crust that is older than 150 million years, so older impact craters would not be preserved anyway. Water absorbs the energy of an impact very effectively, so it would take a very large event to produce even a modest crater on the abyssal plain, and the mobilisation of sediment following an impact would tend to obscure such a signature except in cases where the impactor diameter is comparable to the ocean depth. Presently confirmed ocean impact craters are from shallow-water events only, such as the Mjølnir impact structure north of Norway from the late Jurassic (Tsikalas *et al.* 2002; Tsikalas 2005) and the Montagnais crater off Nova Scotia (Jansa *et al.* 1989; Dypvik & Jansa 2003).

Tsunamis are therefore virtually the only signature of deep-water impacts. Yet evidence for tsunamis from oceanic asteroid impacts is also scarce, and pieces of suggested evidence are fiercely debated (Masse *et al.* 2006; Pinter & Ishman 2008). The known shallow-water impacts of Mjølnir and Montagnais should have left tsunami deposits on nearby shores, yet the search for these has been inconclusive (Dypvik & Jansa 2003; Dypvik *et al.* 2006). In the geological record, only the Chicxulub event (a 100-million-year event) has confirmed associated tsunami deposits, and these were likely produced by massive continental slope failures in the hours or days subsequent to the impact.

Much attention has focused on teletsunamis as being the principal danger from the impact of asteroids with diameters of a few hundred metres (Hills *et al.* 1994; Ward & Asphaug 1994). Others (Crawford 1998; Gusiakov 2007) have urged a more tempered view. We argue, based on numerical simulations, that the tsunami danger for locations far from the impact site is less than the dangers posed by the atmospheric effects of small impacts. Instead, it is the near-field effects that pose the greatest danger in small oceanic impacts, just as in land impacts.

## II. Simulations with the Sage hydrocode

The SAGE hydrocode is a multi-material adaptive-grid Eulerian code with a high-resolution Godunov scheme originally developed by Michael Gittings (Gittings *et al.* 2006) for Science Applications International (SAIC) and subsequently adopted at Los Alamos National Laboratory (LANL). The grid refinement is continuous, cell-by-cell and cycle-by-cycle throughout the problem run. Refinement occurs when gradients in physical properties (density, pressure, temperature, material constitution) exceed user-defined limits, down to minimum cell sizes specified by the user. With the computing power concentrated on the regions of the problem which require higher resolution, very large computational volumes and substantial differences in scale can be simulated at relatively low cost. A variety of

equations of state are available for use with the code, including tabular equations of state from the LANL Sesame library (Holian 1984; Lyon and Johnson 1992) and the SAIC equation of state for water.

We have used the Sage code for simulations of tsunami generation by subaerial and submarine landslides, undersea volcanoes, and earthquakes (Mader and Gittings 2002; Gisler *et al.* 2006a, 2006b; Gisler 2008) and have reported previously on oceanic asteroid impact simulations performed with this code (Gisler *et al.* 2003; Gisler 2007). In these papers we presented calculations of oblique impacts in three dimensions and of vertical impacts in axisymmetric geometry, and demonstrated that the essential features are adequately covered by two-dimensional axisymmetric calculations. The reason for this is that the transient crater is very effectively symmetrised through the vaporisation of water encountered on impact. The kinetic energy per unit mass of an impacting asteroid is many times greater than the latent heat of vaporisation of water, hence many times the asteroid mass will be vaporised on impact. The subsequent development of a propagating wave occurs through the collapse of the transient crater, the formation of a central jet rising many kilometres above the initial water surface, and finally the collapse of that jet and its subsequent rebounds.

The initial waves formed in this manner can be of very high amplitude: substantial fractions, in fact, of the total ocean depth. As such, they are strongly nonlinear; they break in the open ocean over the abyssal plain, and decay rapidly to form trains of much smaller waves. These highly nonlinear waves can be very dangerous to nearby coastlines, but their effects at great distances are more difficult to compute, and have been greatly overstated in the past.

If we define a classical tsunami as a wave with amplitude small compared to the ocean depth and wavelength very much larger than the depth, asteroid ocean impacts do not generate classical tsunamis. Classical tsunamis are generated by undersea earthquakes and landslides, often by dipole couples having lever arms tens to hundreds of kilometres in dimension. The very long waves that are produced can propagate very effectively, with little energy loss, over long distances at the so-called shallow-water speed $\sqrt{gD}$, where $g$ is the acceleration due to gravity and $D$ is the ocean depth. Typical speeds for the waves produced in asteroid ocean impacts are considerably smaller than $\sqrt{gD}$, and the wavelengths of these waves are less than twice the diameter of the transient crater. For example, a 1 km diameter asteroid at vertical impact into a 5 km deep ocean produces a transient crater about 17 km in diameter; the wave that results from the collapse of this crater has a crest-to-crest length that is larger than this by a factor of only 1.5 (this ratio trends slightly larger for smaller impactors). By comparison, the wavelength of the 2004-12-26 Indian Ocean tsunami was ~120 km. The shallow-water speed in this 5 km deep ocean is 221 m/s; the wave produced by the 1 km impact has a speed of 166 m/s.

The calculations we reported for the 2007 Planetary Defense Conference (Gisler 2007) were done for a range of compositions, diameters, and speeds, from 250 m diameter icy bodies to 1000 m diameter iron bodies at speeds from 10 to 20 km/s. All simulation data were eventually collapsed onto curves of wave amplitude versus kinetic energy at various distances from the impact point, from which we concluded that the ocean-wide tsunami danger from likely impactors of less than 500 m diameter was negligible. In this paper we therefore turn greater attention to near-field and atmospheric effects of ocean impacts.

## III. The new calculations

Because the kinetic energy of the impactor was seen to be the most important determinant in our previous work, we decided in this paper to vary only the diameter of the projectile, holding the speed at 20 km/s and using stony densities for all. We extend our diameter range down to 100 m, and include more tracer-particle diagnostics in order to better characterise the waves that are produced, and additionally to help diagnose other near-field effects

The runs reported in this paper are listed in Table 1. Run names, input asteroid diameter, and kinetic energy in Megatons TNT equivalent are the input parameters, followed by outputs of wave characteristics and near-field atmospheric effects. All runs are axisymmetric, computed in a domain of 100 km horizontal extent and 50 km vertical. The vertical space is homogeneously divided into 37 km air (Sesame material #5030, dry air, density 0.00129 g/cc), 5 km ocean (SAIC water, density 1 g/cc), 1 km unconsolidated sediments (Sesame material #7111 alluvium, distended and mixed with water to density ~1.5 g/cc), and 7 km basalt crust (Sesame material #7530, density 2.87 g/cc). The basalt is treated with an elastic-plastic strength model; all other materials in the problem, including the stony asteroid (Sesame material #7391, granite, density 2.63 g/cc) are strength-less. The full domain was initialised in hydrostatic equilibrium. The asteroid was inserted with a downward velocity of 20 km/s at 15 km above the ocean surface in order to preheat the atmosphere above the impact point.

All runs were performed with a minimum resolution of 12.8 cells per projectile diameter. The actual minimum cell sizes varied from 7.8 m for run DwLe to 31.3 m for run DwCe. The runs were performed on an Opteron cluster at the University of Tromsø in Norway, using 32 or 64 processors per run over several weeks. The duration of all runs was

600 seconds physical time (this is the time necessary for a tsunami, initiated at the time of the maximum transient crater for a 1 km impact and travelling at the shallow-water speed of 221 m/s, to exit the 100 km long computational box).

Table 1. Input and output characteristics of oceanic asteroid impact simulations

| | DwCe | DwFe | DwHe | DwIe | DwJe | DwKe | DwLe |
|---|---|---|---|---|---|---|---|
| **Input parameters** | | | | | | | |
| **asteroid diameter (m)** | 1000 | 700 | 500 | 400 | 300 | 200 | 100 |
| **kinetic energy (Megatons TNT eq.)** | 65800 | 22600 | 8220 | 4210 | 1780 | 526 | 66 |
| **transient crater characteristics** | | | | | | | |
| **depth (m)** | 6208 | 5375 | 4375 | 3708 | 3000 | 2208 | 1208 |
| **diameter (km)** | 17.5 | 12.2 | 9.0 | 7.2 | 5.5 | 4.1 | 2.2 |
| **wave characteristics** | | | | | | | |
| **amplitude (m) at 30 km from impact point** | 477 | 285 | 231 | 179 | 133 | 56 | 37 |
| **wave speed (m/s)** | 166 | 160 | 149 | 143 | 138 | 114 | 86 |
| **wavelength (km)** | 28.7 | 20.5 | 17.9 | 15.7 | 13.6 | 9.5 | 4.9 |
| **extent of near-field atmospheric effects, (km)** | | | | | | | |
| **fallout from crown splash** | 67 | 55 | 47 | 36 | 20 | 17 | 7 |
| **hurricane force winds** | 95 | 81 | 75 | 57 | 49 | 36 | 22 |
| **air temperature above 100 C** | 55 | 34 | 26 | 13 | 4 | | |

An illustrative frame from the DwCe run is illustrated in Fig. 1. The wave shown has arisen from the collapse of the central jet, which is at this time undergoing its first rebound. The wave has a leading trough, the last remnant of the transient crater. The crest, over 1.4 km above the initial ocean surface, is breaking. The wave is strongly nonlinear, turbulent, and dissipative. A later stage from the more lightweight DwIe run is shown in Fig. 2. Three wave crests are visible, each from a collapse-rebound cycle of the central jet. The jet collapse and rebound cycle evidently determine the wavelength and period of the waves produced in the impact. In this lower-energy impact, no wave breaking is observed at the scale of these snapshots.

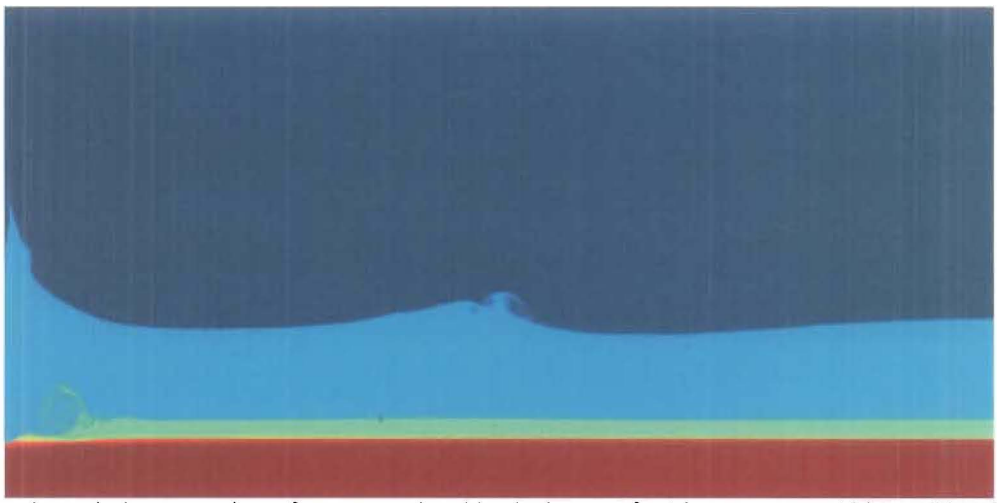

Fig. 1. Snapshot, in vertical cross-section, of a wave produced by the impact of a 1 km stony asteroid into a 5 km deep ocean (run DwCe), 225 seconds after impact. Deep blue is air, cyan is water, green is ocean-bottom sediment (a layer 1 km in thickness), and red is the basalt oceanic crust. The domain illustrated here is from 9 km below sea level to 60 km above, and from the impact point out to 50 km radial distance. The computational domain for all simulations is larger than this window, extending out to 100 km radial distance, down to 13 km below sea level and up to 37 km above. The single wave shown here is 1.4 km high (above original sea level) and breaking. It is preceded by a negative trough of 800 m depth, and the trough-to-crest distance is 8 km. The ocean-bottom sediments have been disturbed in the vicinity of the impact point (at left), and some of this has been lofted in the now-collapsing jet to stratospheric levels. The basalt has been dimpled to 200 m depth over a width of 2.5 km.

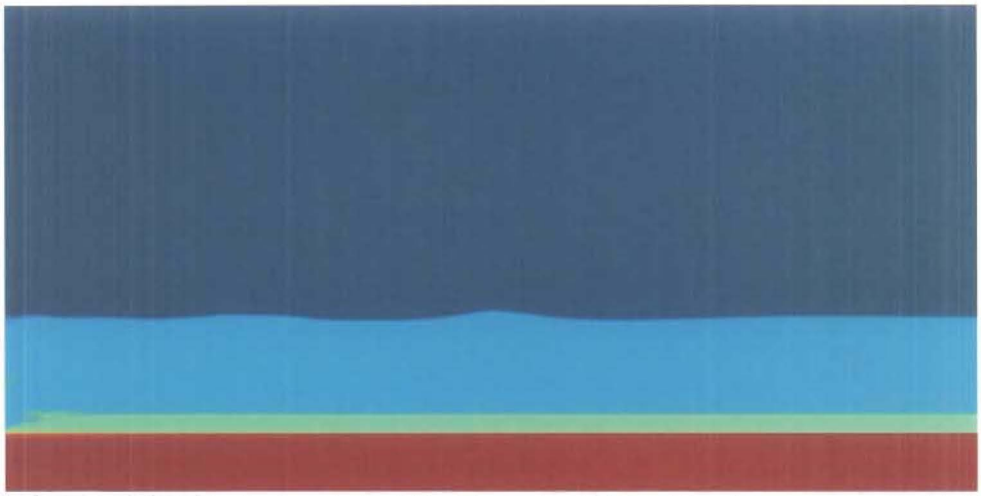

Fig. 2. Snapshot of waves produced by the impact of a 400 m stony asteroid into a 5 km deep ocean (run DwIe), 329 seconds after impact. Colours and geometry are as in Fig. 1. The central wave shown here has a height 275 m above original sea level. There are three detectable wave crests at this time, with crest-to-crest distance 12 km. Though there has been some disturbance of the ocean bottom sediments, there is no dimpling of the basalt beneath. The maximum depth of the transient crater in this case was 1.3 km above the top of the sediment layer, or 3.7 km beneath the original water surface.

Wave characteristics are diagnosed from the trajectories of Lagrangian tracer particles within the simulation domain. In each of these simulations, we placed 150 water surface tracers, evenly spaced along the surface and 50 m above and below, from 1 km out to 50 km from the point of impact. A sample trajectory plot is shown in Fig. 3, for run DwFe. In this plot it is possible to distinguish a lift zone (somewhat larger than the transient crater size), a fallout zone, and a wave zone, partially overlapping. The wave characteristics themselves can be obtained by zooming in on the wave-zone tracers, as shown in Fig. 4 for three vertically offset tracers placed initially 44 km from the impact point in run DwIe. An automated procedure was devised to extract amplitude, period, and wavelength measurements from the 150 tracers used in each run. The procedure required the location of three successive crests and troughs, so particles for which less than three were found were rejected, as were particles with excessive temperatures.

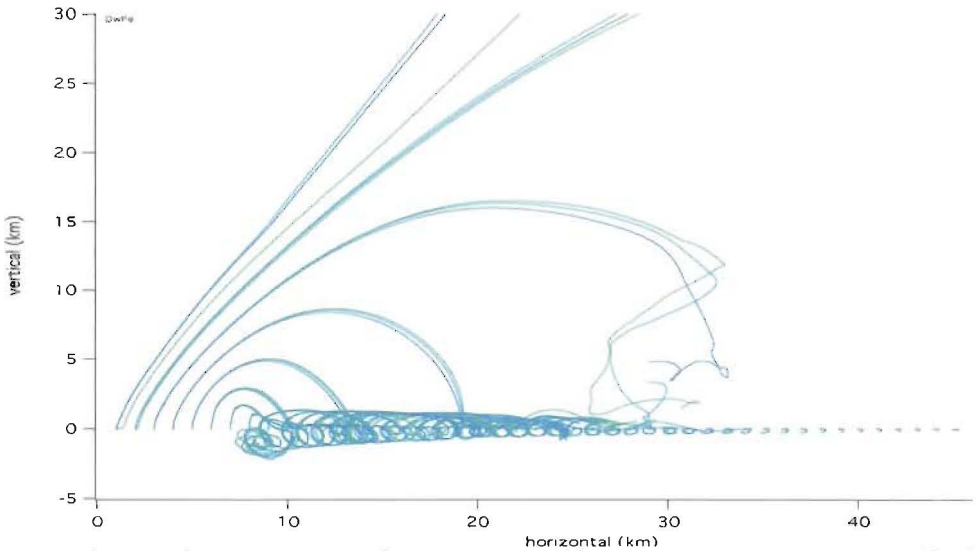


Fig. 3. Trajectory plot of Lagrangian tracer particles from run DwFe (700 m diameter impact). Trajectories for 150 particles are shown; in green are particles that started 50 m above the initial water surface, in cyan those that started on the water surface, and in blue those that started 50 m below. The lift zone is somewhat larger than the transient crater, whose radius is 6.1 km; and the pure wave zone begins around 25 km. The fallout zone, as seen in this figure, goes out to at least 32 km; from analysis of other tracers, placed below the water surface within the transient crater and omitted here, the fallout zone extends out to 55 km.

Sample plots of amplitude against distance, and of distance against time for three successive wave crests, are shown in Fig. 5 for run DwIe. The wave amplitude decays with distance, rapidly at first because of wave breaking and other

nonlinear effects, and subsequently more slowly. We have not followed waves in these calculations beyond slightly more than 50 km, but we obtain approximate power-law decays at that distance with index -0.7 for all impactors.

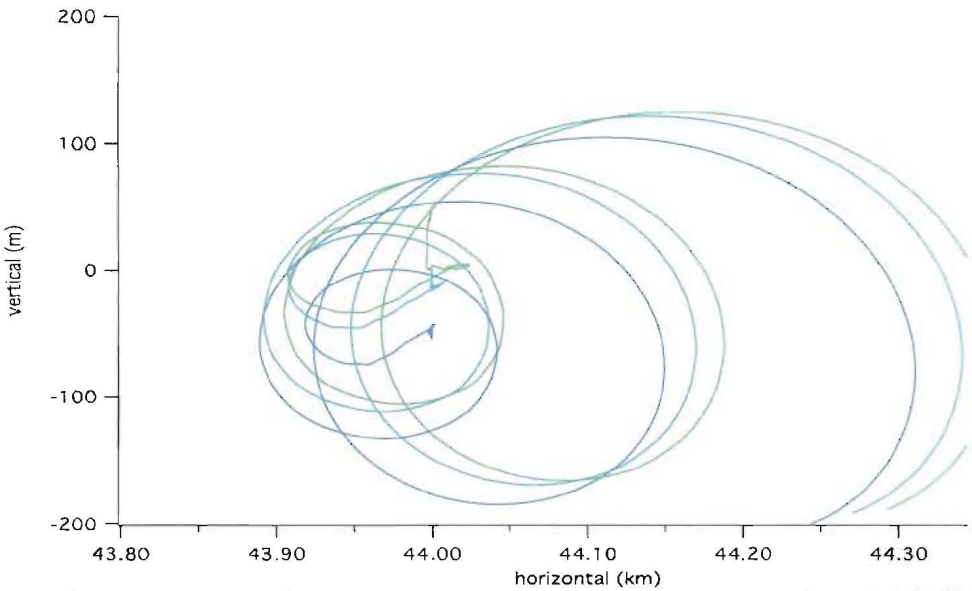


Fig. 4. Trajectory plot for three vertically offset tracers in run Dwle (400 m diameter impact). After a period of initial drift, these three particles are hit by the initially regressive wave from the decay of the transient crater, and are then taken in three successive oscillations about a centre that drifts away from the impact site. In this case each of the three oscillations is of greater amplitude (vertical and horizontal) than the previous. For some other particles the first or the second oscillation is larger. These particular tracers have a smooth motion that is easy to follow; most (see Fig. 6) do not.

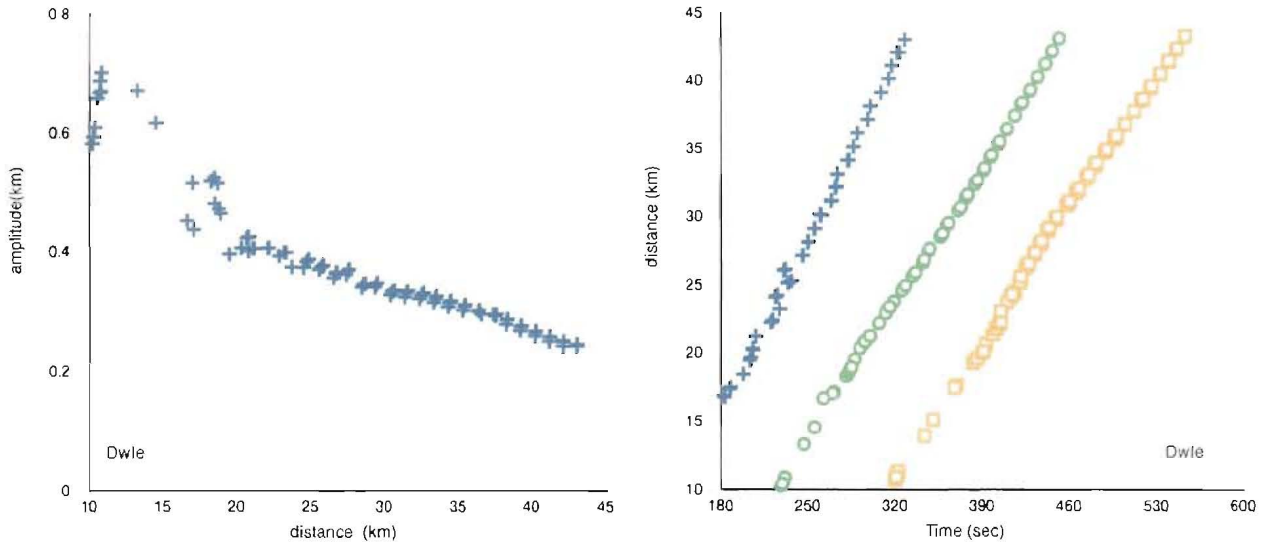


Fig. 5. Wave amplitude as a function of distance from the impact point (left) and distance from the impact point as a function of time for three successive wave crests (right) for run Dwle, the 400 m diameter impact. These were obtained from analysis of 92 tracer particle trajectories from the original 150 water-surface tracers placed in this run. The tracers that were eliminated from the analysis were those that had fewer than three successive crests and troughs within the 600 seconds of the simulation, and those with excessive temperatures. Plots like these were generated for all runs, and the wave characteristics listed in Table I were obtained from these.

To illustrate the difference between classical tsunamis and asteroid impact waves, in Fig. 6 we show a comparison of tracer-particle plots from run DwHe and a run done for a study (by ourselves but still in progress) of a tsunami produced by the prehistoric El Golfo landslide from the island of El Hierro in the Canaries (Masson 1996). These two simulations are comparable to one another in terms of the available free energy. For DwHe, this free energy is the

kinetic energy of the asteroid, 8.2 Gigatons, and for the El Golfo run it is the difference in gravitational potential energy between the initial position of the slide mass and its final position, ~7.9 Gigatons (taking ~250 km$^3$ as the slide volume, an average density of 2.7 g/cc, and translating it down by ~5 km to the seafloor).

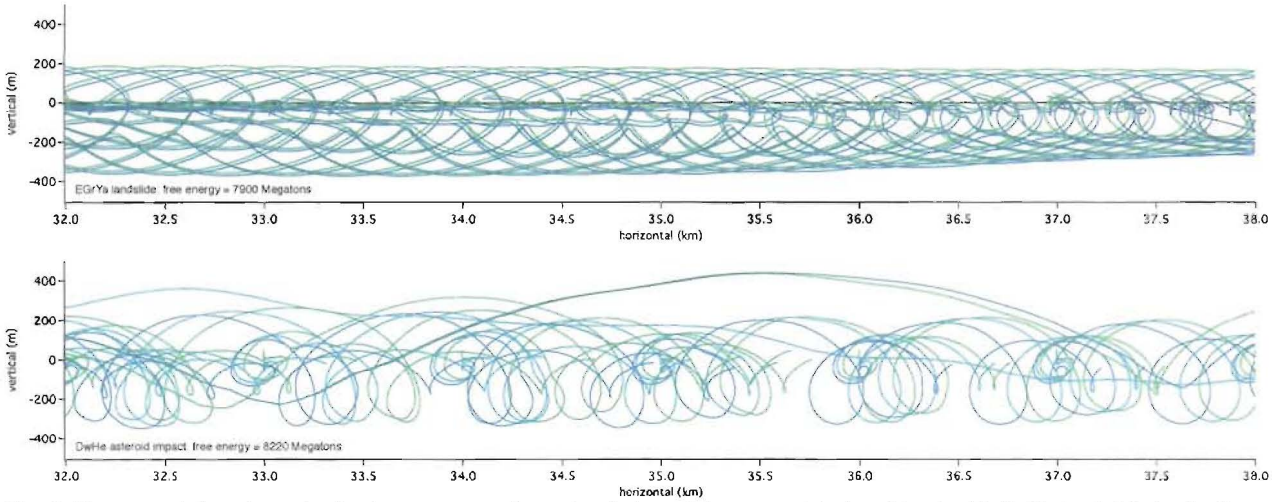


Fig. 6. Tracer particle trajectories in the wave zone for a simulation of the tsunami induced by the El Golfo landslide in the Canary Islands (top) and for the wave produced by the impact of a 500 m diameter asteroid (run DwHe, bottom). These events are of comparable source energy.

The difference between particle trajectories in the El Golfo simulation (top panel) and the asteroid impact simulation (bottom panel) could hardly be more striking. The particle motion in the top panel is orderly, with each particle's motion closely resembling that of its neighbours. The coupling of rock motion to water motion occurs at speeds slow compared to the speed of sound in either medium, and a coherent wave is produced. The much more violent collision between rock and water that occurs in an asteroid impact at hypersonic speed has produced considerably more disorder in the bottom panel. Many of the particles have trajectories that are partly wave-like, but they are jerked from one mode to another as the complex and turbulent wave train passes. At least four particles in this panel are on very long looping trajectories that originated within the fallout zone, less than 15 km from the impact point. These are moving at *particle* speeds up to 200 m/s, comparable to the wave speed. Normally, particles participating in transverse wave motion have particle speeds much less than the wave speed, and particle oscillation lengths much smaller than the wavelength. This is the case for all particles in the top panel.

If we apply the same analysis to the El Golfo tracers as we applied to the asteroid impact tracers, we get a wavelength of ~40 km and a wave speed of ~170 m/s. These numbers are consistent with the interpretation of this wave structure as a classical tsunami. The water depth 35 km from El Hierro is 3.3 km, giving a shallow-water-wave speed of 178 m/s. On the other hand, the wave speed in DwHe is ~150 m/s, inconsistent with the shallow-water wave speed of 221 m/s in the 5 km deep ocean, and the wavelength of 18 km is only slightly more than 3 times the depth. This asteroid impact wave structure is not a classical tsunami.

## IV. The dangers from oceanic asteroid impacts

We argue here, as we have previously done, that the long-distance tsunami danger from the impact of a (say) 200 m diameter asteroid is not as great as others have supposed. Such impacts do not produce classical tsunamis; the waves they produce are of shorter length and lower speed. They are more disorderly and chaotic, will decay more rapidly, and will not propagate efficiently over long distances. Nevertheless, the prospect of such an impact is not to be taken lightly.

An impact of a 200 m stony body at 20 km/s releases energy equivalent to a > 500 Megaton nuclear device, whether on land or on water. If this occurs in or near a populated region, millions would die. If this occurs in an unpopulated region, whether in the middle of the Pacific or in the middle of the Sahara desert, it might lead to thousands of deaths and produce serious climate effects that could last for years or decades. But it will not produce a global tsunami of unprecedented size and devastation.

The real dangers from water impacts are mainly atmospheric. The most immediate of these are concentrated in the near field, just as for land impacts. The extent of the near-field effects is shown in Fig. 7. These immediate dangers include the blast wave from the explosive vaporisation of water, followed by hurricane force winds out to tens of kilometres and

high temperatures over similar distances. For impactors of diameters greater than 500 m, air temperatures may exceed the boiling point of water over tens of kilometres. The fallout zone, where water excavated from the transient crater falls back to the surface in enormous quantities at terminal velocity extends out to 50 km for a 500 m asteroid impact. An impact in deep water close to a narrow continental shelf (as on the west coast of the Americas or the east coast of Asia) could produce massive destruction from this fallout.

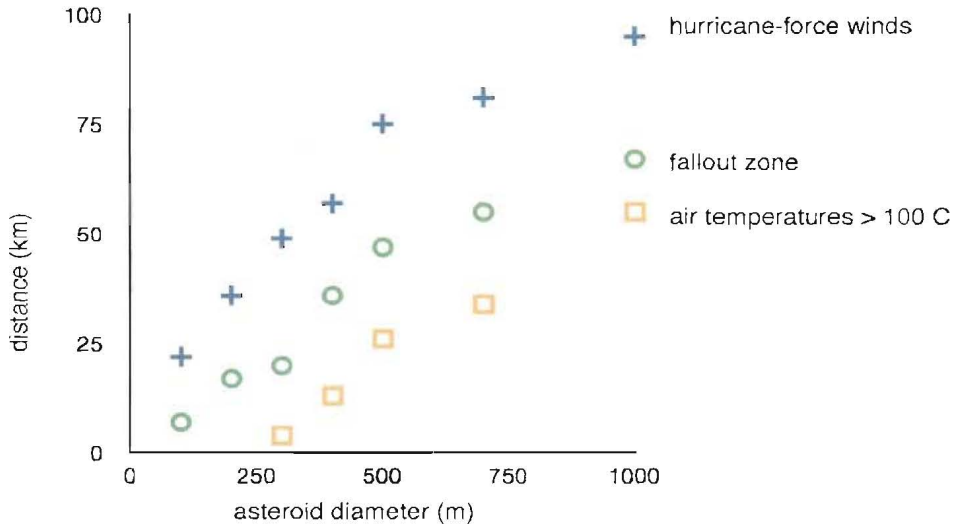


Fig. 7. Extent of near-field effects for the asteroid impact simulation runs of Table 1. In the axisymmetric simulations, the winds shown circulate outward close to the surface and back at altitude. On Earth these would probably generate cyclonic flows. The fallout zone is where water, expelled in the crown splash as the transient crater forms, falls back to the surface at terminal velocity. Any structures in this region would be destroyed. The high temperatures generated in the blast wave from the initial impact extend to tens of kilometers for impactors greater than 400 m diameter.

Deep-water tracers in the initial area of the transient crater show us where the excavated water goes. Very preliminary analysis of the deep water tracers in the DwKe run suggests that, of the 58 Gigatonnes of water excavated in this impact, roughly a third is catapulted into the stratosphere above 20 km altitude, another third is shoved out laterally, and a final third is splayed out in the crown splash to come down to earth in the fallout zone. In DwKe, the fallout zone extends out to 17 km; if the fallout occurs evenly throughout this zone, every square metre would receive 22 tonnes of water. This water is falls at speeds of 100-300 m/s: if there are any buildings standing in this zone, they would be severely damaged.

The near-field effects illustrated in Fig. 7 extend out to 100 km from the point of impact and can be deadly for affected populations. Some 2 to 5 % of the ocean surface lies within 50 to 100 km of continental land masses, and a considerably greater fraction lies within a similar distance of populated islands. These admittedly local effects are probably the most important immediate dangers from ocean impacts of asteroids smaller than 1 km in diameter.

The water injected into the stratosphere has consequences of a more serious long term and global nature. The stratosphere is mostly dry; most of Earth's water vapour is in the troposphere and cycles fairly rapidly (days to weeks) back to the ground. Its residence time in the stratosphere is considerably longer, on the order of decades. Water vapour is an important greenhouse gas: the 20 Gigatonnes injected into the stratosphere in the DwKe run, although only 0.1% the total water content of the troposphere, is a factor of 100 greater than the present-day water vapour of the stratosphere (Rosenlof *et al.* 2001). Because of the much longer residence time in the stratosphere, such an injection may have serious implications for the global climate. Much greater quantities of water are injected into the stratosphere for larger impacts, and for a 1 km object may exceed the total water content of the present atmosphere. Whether such a sudden injection of water would lead to a warming (because of greenhouse effects) or a cooling (because of the formation of albedo-increasing ice clouds in the stratosphere) is beyond the scope of this study.

## V. Conclusions

We have performed numerical calculations of deep-water impacts to understand wave generation and energy deposition from these events. We have used tracer particles to measure the characteristics of asteroid impact waves, and find them to be of shorter period and wavelength than expected for tsunamis. The waves are disorderly, and subject to dissipation

and decay. We have further examined near-field effects from such impacts, and find that these mainly atmospheric effects can be deadly up to 100 km away from the impact point. In addition the injection of water vapour into the stratosphere may have serious consequences for climate that may last years or decades.

The question concerning the planetary defence community is: What is the minimum size asteroid we need to defend Earth against? Based on the work presented here, the ocean impact of an asteroid of size less than about 500 m in diameter will not lead to a global catastrophe, though it could cost millions of lives if it landed in the wrong place.

Acknowledgments

We gratefully acknowledge the support of the Norwegian Research Council for the establishment and funding of the Centre for the Physics of Geological Processes, a Norwegian Centre of Excellence in Research at the University of Oslo. The computing reported here has been done mostly through resources provided by NOTUR, the Norwegian distributed supercomputing network.

References

D.A. Crawford. Modeling asteroid impact and tsunami, *Science of Tsunami Hazards*, **16**, 21-30 (1998).

H. Dypvik, L. F. Jansa. Sedimentary signatures and processes during marine bolide impacts: a review, *Sedimentary Geology* **161**, 309-337 (2003).

H. Dypvik, M. Smelror, P.T. Sandbakken, O.Salvigsen, and E. Kalleson. Traces of the marine Mjølnir impact event, *Palaeogeography, Palaeoclimatology, Palaeoecology*, **241**, 621-636 (2006).

G Gisler, R Weaver, C Mader, M Gittings. Two and three dimensional simulations of asteroid ocean impacts, *Science of Tsunami Hazards*, **21**, 119 (2003).

G Gisler, R Weaver, M Gittings, "Sage Calculations of the tsunami threat from La Palma", *Science of Tsunami Hazards*, **24**, 288-301 (2006a).

G Gisler, R Weaver, M Gittings, "Two-dimensional simulations of explosive eruptions of Kick-em Jenny and other submarine volcanos", *Science of Tsunami Hazards*, **25**, 34 (2006b).

G. Gisler. Tsunamis from asteroid impacts in deep water, *Planetary Defense Conference 2007,* at http://www.aero.org/conferences/planetarydefense/2007papers.html (2007).

G. Gisler. Tsunami simulations, *Annual Review of Fluid Mechanics*, **40**, 71-90 (2008).

M.L. Gittings., R.P. Weaver, M. Clover,, *et al.*, 2006. The RAGE radiation-hydrodynamic code, *Los Alamos National Laboratory Report LA-UR-06-0027*, Los Alamos, New Mexico.

V.K. Gusiakov. Tsunami as a destructive aftermath of oceanic impacts, in *Comet/asteroid impacts and human society*, ed. P.T. Bobrowsky & Hans Rickman, Springer, pp 247-263 (2007).

J.G. Hills, I.V. Nemchinov, S.P. Popov, A.V. Teterev. Tsunami generated by small asteroid impacts, in *Hazards due to comets and asteroids*, ed. T. Gehrels, University of Arizona Press, pp 779-790 (1994).

K.S. Holian, 1984. T-4 Handbook of material properties data bases: Vol 1c, equations of state, *Los Alamos National Laboratory Report LA-10610-MS*, Los Alamos, New Mexico.

L.F. Jansa, G. Pe-Piper, P.B. Robertson, and O. Freidenreich. Montagnais, a submarine impact structure on the Scotian Shelf, eastern Canada. *Geological Society of America Bulletin* **101**, 450-463 (1989).

S.P. Lyon, J.D. Johnson, 1992, Sesame: the Los Alamos National Laboratory equation of state database, *Los Alamos National Laboratory Report LA-UR-92-3407*, Los Alamos, New Mexico.

C. L. Mader and M. L. Gittings. Modeling the 1958 Lituya Bay mega tsunami II, *Science of Tsunami Hazards* **20**, 241-250 (2002).

W. Masse, E. Bryant, V. Gusiakov, D. Abbott, G. Rambolamana, H. Raza, M. Courty, D. Breger, P. Gerard-Little, L. Burckle. Holocene Indian Ocean cosmic impacts: The megatsunami chevron evidence from Madagascar, *EOS Trans. AGU*, **87(52)**, Fall Meet. Suppl. Abstract PP43B-1244 (2006).

D.G. Masson, Catastrophic collapse of the volcanic island of Hierro 15 ka ago and the history of landslides in the Canary Islands, *Geology* **24**, 231-234 (1996).

N. Pinter, S.E. Ishman. Impacts, megatsunami, and other extraordinary claims, *GSA Today*, **18**, 37-38 (2008).

K.H. Rosenlof, S.J. Oltmans, D. Kley, J.M. Russell III, E-W. Chiou, W.P. Chu, D.G. Johnson, K.K. Kelly, H.A. Michelsen, G.E. Nedoluha, E.E. Remsberg, G.C. Toon, M.P. McCormick. Stratospheric water vapor increases over the past half-century, *Geophysical Research Letters*, **28**, 1195-1198 (2001).

F. Tsikalas, S. T. Gudlaugsson, J. I. Faleide, and O. Eldholm,.The Mjølnir marine impact crater porosity anomaly, *Deep-Sea Research II* **49**, 1103-1120 (2002).

F. Tsikalas Mjølnir Crater as a result of oblique impact: asymmetry evidence constrains impact direction and angle. In *Impact Studies (Impact Tectonism)*, edited by Koeberl C. and Henkel H. Berlin-Heidelberg: Springer Verlag. pp. 285-306 (2005).

S.N. Ward, E. Asphaug. Asteroid impact tsunami: a probabilistic hazxard assessment, *Icarus* **145**, 64-78 (2000).